Optical Parametric Oscillator Longitudinal Modes Suppression Based on Smith Predictor Control Scheme

Ali Salehiomran, Rahi Modirnia, Benoit Boulet, and Martin Rochette

***Abstract*— Fiber optical parametric oscillators (FOPOs) contain multiple longitudinal modes arising from the hundreds of meters to a kilometer scale length of their cavity. To obtain better understanding of the longitudinal modes and to find out how to suppress them, a model for the operation of FOPOs is introduced. This model utilizes the sinusoidal-input describing function (SIDF) as a quasi-linear approximation of the nonlinear dynamics of parametric amplification. Applying this model, the SIDF of the FOPO is derived, which predicts that the origin of the longitudinal modes is the presence of the cavity round-trip delay term in the characteristic equation (the denominator) of the transfer function. To eliminate the effect of the delay term, a modified Smith predictor control scheme has been applied to the FOPO cavity, and a control algorithm is developed. This algorithm has been numerically analyzed and experimentally implemented, where the results indicate drastic suppression of the longitudinal modes.**

***Index Terms*— Fiber optical parametric oscillator (FOPO), longitudinal modes, sinusoidal-input describing function (SIDF), Smith predictor.**

I. Introduction

FIBER optical parametric amplifiers and oscillators (FOPAs, FOPOs) have attracted widespread interest because of their potential applications in optical signal processing and optical fiber communication systems [1]. Their applications include ultrafast all-optical signal sampling, high-repetition rate pulse train generation, and time division multiplexing [2]. In particular, FOPOs are capable of generating coherent light with broad continuous wavelength tunability [3], [4]. They convert a fixed laser source into a tunable laser source. This conversion takes place inside a feedback loop (the resonant cavity) containing a nonlinear medium. Light confined in the cavity reflect multiple times producing standing waves at certain resonance frequencies. The standing wave patterns produced are called longitudinal modes [5]. The required length of the nonlinear medium depends on its constitutive material. Silica-based fibers are mostly used as the nonlinear medium and their length is in the order of several hundreds of meters [6], [7]. As a result, the spacing between the longitudinal modes is in the order of several hundreds of kHz. With the typical optical filter having a bandwidth of several tens of GHz, the longitudinal modes of such a laser cavity cannot be filtered down to single mode. Consequently, FOPOs due to their large cavity length are multimode laser sources. The output power from a multimode FOPO suffers from noisy intensity fluctuations [5]. Thus, it is desired to suppress the longitudinal modes of the FOPO as much as possible and achieve single longitudinal mode operation.

Various approaches have been applied to achieve single longitudinal modes (SLM) operation [8]–[10]. A fiber loop mirror with Erbium-doped fiber (EDF) as a saturable absorber has been proposed to attain SLM operation in [8]. In [9], SLM operation is achieved by a high finesse fiber Bragg grating (FBG). In another approach, a multiring cavity is applied to obtain SLM operation [10]. The EDF as a saturable absorber comes with a major drawback that the useful spectral range is limited to the absorption spectrum of the EDF (1530–1570 nm). Applying a high finesse FBG restricts the tuning range of the laser to $<$10 nm [9]. Approaches based on multiring cavities require few centimeters long loops or fiber Fabry-Perot tunable filter (FFP-TF) to obtain GHz order free spectral range (FSR) and force SLM operation.

In this brief, we introduce and experimentally demonstrate a multiring cavity structure to suppress the longitudinal modes of FOPOs. In contrary to other structures of longitudinal modes suppression, this structure is applicable to arbitrary wavelengths. Thus, this structure is considered as a prominent candidate to suppress longitudinal modes at unconventional wavelengths (e.g., 2–5 μm), where other methods are not applicable. In addition, this structure does not require few centimeters long loops or FFP-TF. Therefore, in comparison with other methods the complexity and cost of design are reduced. The control strategy used in this structure is the Smith predictor scheme, which is a model-based internal control technique and has been specifically designed to address delay in closed-loop system [11]. The Smith predictor technique is of interest in this application, because multiple longitudinal modes originate from the propagation delay inside the cavity of FOPO. Since the Smith predictor technique is specifically designed for delayed-systems, it overcomes the propagation delay of the cavity and suppresses longitudinal modes. The Smith predictor utilizes the model of the dynamic behavior of the system to deal with time delays in the system, eliminating the delay term in the denominator of the overall closed-loop transfer function.

The rest of this brief is organized as follows. In Section II, the problem of the longitudinal modes and their origin is thoroughly discussed. Then in Section III, a quasi-linear model of the dynamics of the FOPO based on the sinusoidal-input describing function (SIDF) is established. The Smith

Manuscript received February 19, 2013; revised August 1, 2013; accepted October 28, 2013. Manuscript received in final form November 4, 2013. Date of publication November 20, 2013; date of current version July 24, 2014. Recommended by Associate Editor A. G. Alleyne.

The authors are with the Department of Electrical and Engineering, McGill University, Montreal, QC H3A 0E9, Canada (e-mail: alisalehiomran@gmail.com; rahi@cim.mcgill.ca; benoit.boulet@mcgill.ca; martin.rochette@mcgill.ca).

Color versions of one or more of the figures in this paper are available online at http://ieeexplore.ieee.org.

Digital Object Identifier 10.1109/TCST.2013.2289934

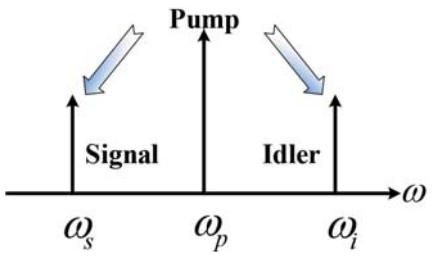

Fig. 1. Frequency assignment of the degenerate (one-pump) FWM.

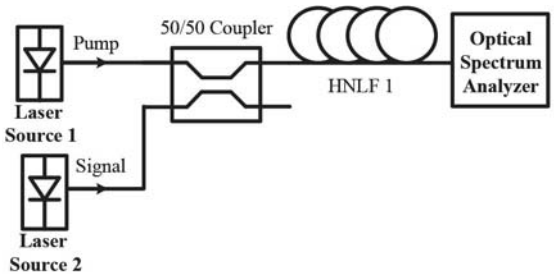

Fig. 2. Schematic of the experimental setup for the realization of a FOPA and measuring the parametric gain (HNLF).

predictor scheme is introduced in Section IV, and is applied to the developed model of the system in Section V, after which the block diagram of the system is obtained, and the closed-loop transfer function of the system is derived. The control algorithm is developed in Section VI. In Section VII, the designed controller is then tested on the system as the closed-loop system is numerically analyzed in MATLAB to examine the functionality and performance of the proposed method. Finally, in Section VIII, to verify the validity of the results, the closed-loop system is experimentally implemented.

II. Description of the Problem

The operation of FOPAs and FOPOs is based on Kerr nonlinearity that arises from the intensity dependence of the refractive index. Kerr nonlinearity results in various nonlinear phenomena among which four-wave mixing (FWM) is the source of parametric gain inside optical fibers [12]. As the name FWM suggests, in this nonlinear phenomenon four optical waves at different frequencies are coupled together in a nonlinear fashion. Degenerate FWM is a special case, where two of these frequencies coincide. Fig. 1 shows the frequency assignment of the degenerate or one-pump FWM. Consider three optical waves, namely a pump, signal and idler, oscillating at frequencies ω_p, ω_s, and ω_i, respectively. A pump laser is a continuous wave (CW) laser source that supplies energy for the FWM process. Generally, pumps have more power than the signal as presented in Fig. 1 by the length of the arrows. As the signal co-propagates with the pump inside the nonlinear medium, energy is transferred from the pump to the signal resulting in amplification of the signal. At the same time, a new wave (idler) is generated following the rule of energy conservation [2], [12]

$$\omega_s + \omega_i = 2\omega_p. \tag{1}$$

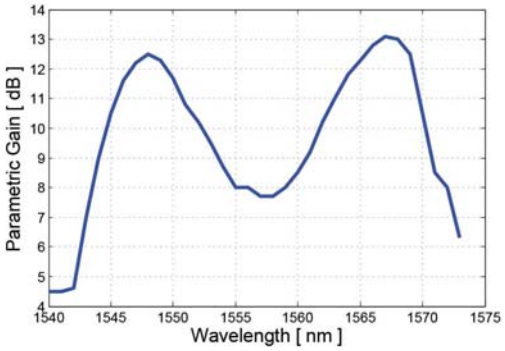

Fig. 3. Experimental measurement of the parametric gain-spectrum using the setup shown in Fig. 2. HNLF has nonlinearity coefficient of $\gamma = 13\ \mathrm{W^{-1}km^{-1}}$ and propagation length of $L = 1$ km. The pump power at the input of HNLF is 200 mW.

The amount of parametric gain is proportional to the length of the nonlinear medium (interaction length of the waves), the nonlinearity of the medium represented by the nonlinearity coefficient γ, and the power of the pump. Momentum conservation is the other criteria that limit the bandwidth of the gain-spectrum. Hence, gain is observed over a limited bandwidth [12].

Fig. 2 shows a setup for the demonstration of parametric amplification. In our experiment, a silica-based highly nonlinear fiber (HNLF) with the nonlinearity coefficient of $\gamma = 13\ \mathrm{W^{-1}km^{-1}}$ is used as a gain medium. The signal is amplified inside the HNLF due to FWM and a FOPA is realized. A CW laser source at the wavelength of 1557 nm with the power of 200 mW is used as a pump. The pump is combined equally to a tunable laser signal by means of a 50/50 optical coupler. An optical coupler combines two optical input fields by a certain power coupling ratio and delivers two optical output fields. A 90/10 optical coupler delivers 90% of the power the first input plus 10% of the power of the second input at the first output. Similarly, 10% of the power of the first input plus 90% of the power of the second input are delivered at the second output. As shown in Fig. 2, the output of the coupler, which is combined pump and signal, is sent into the HNLF. FWM takes place inside the HNLF, and as a result, the signal is amplified. Fig. 3 shows an experimental measurement of the parametric gain. Due to momentum conservation criteria, the gain-spectrum has a limited bandwidth [12].

Fig. 4 depicts the schematics of a typical FOPO. A pump laser at wavelength λ_P is supplied externally and passes through a feedback loop composed of a HNLF, a bandpass filter (BPF), three optical couplers C, C_5, and C_6, and two connecting fibers L_2 and L_3. While propagating inside the nonlinear medium, the pump provides gain to every signal inside its gain-spectrum via FWM. The amplified spectrum is filtered by the BPF at the central wavelength λ_S, which sets the operation wavelength. The couplers C and C5 serve to inject the pump in the cavity, sample the circulating signal, and close the feedback loop. Optical power in the cavity builds up into a laser oscillation once the gain at the operation wavelength equals or exceeds the net loss of the cavity. Insertion loss of the HNLF, BPF, and optical couplers are the main sources of loss

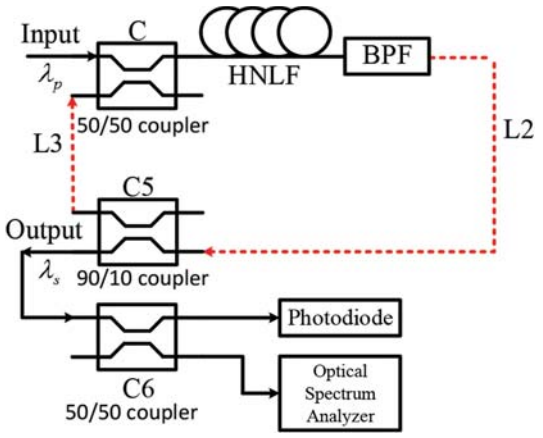

Fig. 4. Schematic of the experimental setup used to implement a FOPO. HNLF, BPF, C, C_5, and C_6 represent optical couplers, and L_2 and L_3 represent connecting fibers.

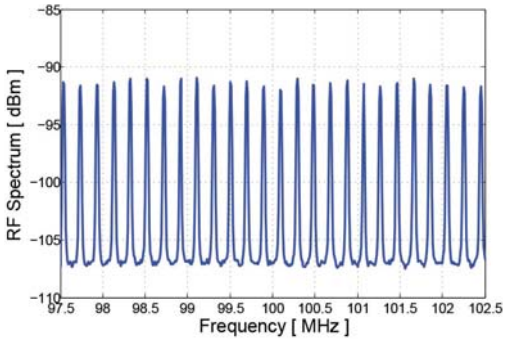

Fig. 5. Measured RF spectrum of the output of FOPO of Fig. 4. Due to the propagation length of the medium (1 km), the mode spacing among longitudinal modes is 200 kHz.

inside the cavity. By means of a 90/10 optical coupler (C_6), 10% of the power of the signal circulating inside the cavity is sampled and is divided into two branches. One branch is fed into the optical spectrum analyzer (OSA) and the other one goes into a photodiode. OSA shows the spectrum of the signal around the optical carrier. The resolution of OSA (Agilent 86142B) is ~6 GHz around the carrier at the wavelength of 1550 nm or the frequency of 193 THz. The output of the photodiode is proportional to the input intensity fluctuations. Thus, the photodiode converts the optical power into an electrical signal amplitude. In this process, the optical carrier is omitted, therefore a 1 kHz resolution is achievable [13]. To observe the longitudinal modes, the laser output is sent to a 45 GHz photodiode (U2TBPDV2020R) and then to an RF spectrum analyzer. OSA provides the big picture, while the RF spectrum analyzer provides the detailed spectrum around the frequency of operation.

Fig. 5 shows the RF spectrum of the output of the FOPO of Fig. 4. It is observed that the frequency spacing among the longitudinal modes, also known as FSR, is 200 kHz. This is in agreement with the theoretical expectations [5]

$$\mathrm{FSR} = \frac{c_0}{nL} \tag{2}$$

where L is the length of the FOPO cavity, n is the refractive index of the propagation medium, and c_0 is the speed of light

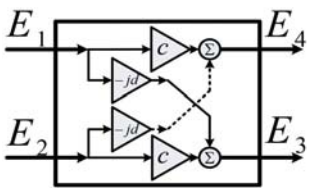

Fig. 6. Block diagram of an optical coupler. c and d represent throughput and cross-path coupling coefficients.

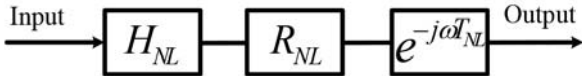

Fig. 7. Block diagram of the nonlinear model of the HNLF and BPF. H_{NL} represents the SIDF of the nonlinear processes. R_{NL} and T_{NL} denote the loss and propagation delay of the HNLF and BPF.

in vacuum. In the experimental setup shown in Fig. 4, the cavity length is 1 km, and the refractive index is 1.5. Consequently, the mode spacing calculated from (2) is 200 kHz. This narrow frequency spacing leads to the fact that many of these modes pass through the BPF (typical bandwidth of 50 GHz).

Parametric oscillation in nature is a nonlinear process. The role of the nonlinear processes inside a FOPO cavity is to provide gain. To analyze the effects of the nonlinear element, a model of the linear part of the FOPO cavity is required. In the Section III, after the derivation of this model in the vicinity of the operation frequency, the block diagram of the FOPO system is obtained and the closed-loop SIDF is derived [14]. This transfer function, which includes the nonlinearity of the parametric amplification, predicts the closed-loop dynamics.

III. Nonlinear Model of FOPO

To obtain a model for the operation of the FOPO shown in Fig. 4, models for HNLF, optical connecting fibers, and optical couplers are required. Fig. 6 shows the equivalent block diagram of an optical coupler. The two input fields E_1 and E_2 are related to the two output fields E_3 and E_4 by a coupled equation [15]

$$\begin{bmatrix} E_4 \\ E_3 \end{bmatrix} = \begin{bmatrix} c & -jd \\ -jd & c \end{bmatrix} \begin{bmatrix} E_1 \\ E_2 \end{bmatrix} \tag{3}$$

where c and d denote the throughput and cross-path coupling coefficients, respectively. Fig. 7 shows the nonlinear model of the HNLF and BPF. In this model $H_{\mathrm{NL}} = \sqrt{G_{\mathrm{NL}}} e^{-j\Phi_{\mathrm{NL}}}$ refers to the SIDF of the nonlinear processes [14], G_{NL} and Φ_{NL} are the nonlinear gain and phase shift [16], R_{NL} is the insertion loss of the nonlinear medium and BPF, T_{NL} is the propagation delay of the nonlinear medium and BPF. Fig. 8 shows the equivalent block diagram of a connecting optical fiber, such as L_2 and L_3. This model consists of a loss element denoted by R_i and a propagation delay element denoted by T_{Li}.

Fig. 9 shows the block diagram of the FOPO in a conventional feedback structure. This model is valid only at the wavelength of operation (λ_s) established by the BPF. In this model H_{NL}, R_{NL}, and T_{NL} represent nonlinear processes as introduced in Fig. 7, and R_2, R_3, T_{L2}, and T_{L3} represent

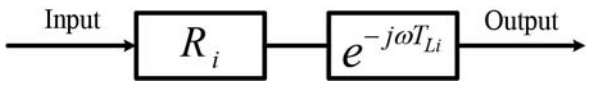

Fig. 8. Block diagram of a connecting optical fiber. R_i, and T_{Li} denote the loss and propagation delay of a connecting optical fiber.

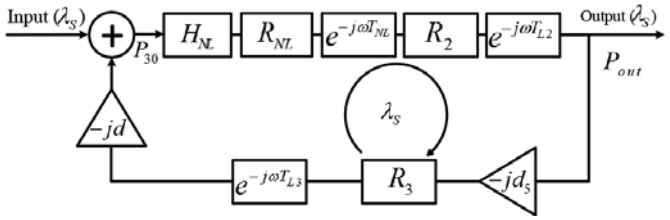

Fig. 9. Block diagram of a FOPO in the vicinity of the operation frequency (λ_s), in a conventional feedback structure.

the insertion losses and propagation delays of the connecting fibers. The input to output transfer function becomes [16]

$$H(j\omega) = \frac{B_1 e^{-j\omega(T_{\mathrm{NL}}+T_{L2})}}{1 - B_2 e^{-j\omega(T_{\mathrm{NL}}+T_{L2}+T_{L3})}} \tag{4}$$

where $B_1 = H_{\mathrm{NL}}(\omega)R_{\mathrm{NL}}(\omega)R_2$, and $B_2 = H_{\mathrm{NL}}(\omega)R_{\mathrm{NL}}(\omega)R_2R_3dd_5$. As (4) implies, the origin of the longitudinal modes is the existence of the delay term at the characteristic equation. Therefore, there is a need for a time-delay compensation control method to eliminate the longitudinal modes or increase the spacing between successive modes. There are several time-delay compensation methods, one of the most important of which is the Smith predictor method.

IV. Smith Predictor Control Technique

To compensate for time delays in a system, several control strategies have been proposed to improve the performance of the closed-loop system. One of the best known and most effective strategies is the Smith predictor control method. It is proven that the performance of a controller incorporating the Smith predictor is better than a conventional type controller [17]. Fig. 10 shows the block diagram of the Smith predictor control structure [11].

To use the Smith predictor control method, the modeled dynamics of the actual system needs to be derived. The model of the actual system has to be separable into two sections of delayed and un-delayed dynamics of the system. The model of the system is $H_{\mathrm{est}}(j\omega)$ and is described by $H_{\mathrm{ud}}(j\omega)e^{-j\omega T}$, where $H_{\mathrm{ud}}(j\omega)$ represents the part without the delay, and $e^{-j\omega T}$ represents the time-delay of the system. The idea of incorporating the Smith predictor technique is to have the controller act on the undelayed part of the system so it can provide a faster reaction to the changes in the system, resulting in improved tracking of the input. In other words, the Smith predictor masks the delay of the system for the controller, so that the controller acts more efficiently [17]. Fig. 11 depicts the equivalent block diagram of the Smith predictor technique in a conventional type feedback loop. The implementation of the Smith predictor in the conventional type feedback loop shown in Fig. 11 is more practical in photonics environment, thus this version is applied to the FOPO system.

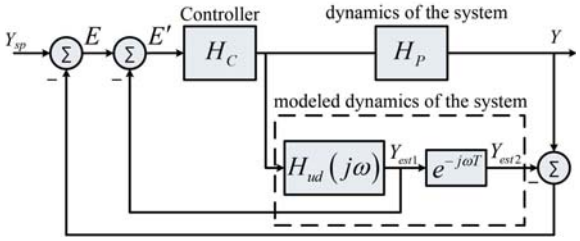

Fig. 10. Block diagram of the Smith predictor control scheme.

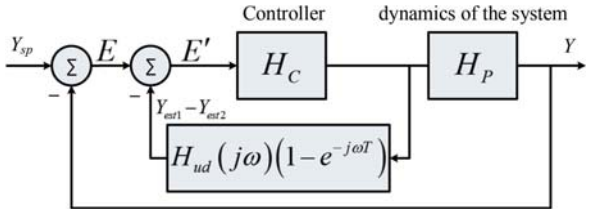

Fig. 11. Block diagram of the Smith predictor technique in a conventional type feedback loop structure.

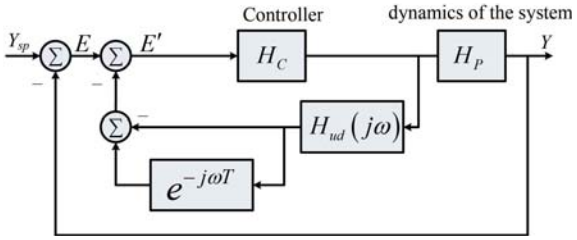

Fig. 12. Block diagram of the Smith predictor technique in a conventional type feedback loop structure with focus on inner feedback loop.

V. Application of the Smith Predictor Control Technique to the FOPO System

Fig. 12 shows the block diagram of the conventional type Smith predictor feedback loop structure with focus on inner feedback loop. To apply the Smith predictor control method to the FOPO system, there have to be slight modifications applied to this structure due to limitations in implementation of the control algorithm in a practical optical setup. Fig. 13 shows the block diagram of the modified Smith predictor technique system applied to the FOPO system. In this structure, the order of appearance of the plant and controller has changed. This is to avoid influencing the nonlinear gain of the HNLF in the actual physical implementation of the system. Since this system is a single input single output system, the order of appearance of the plant and controller does not matter in a mathematical sense. Comparing Figs. 12 to 13, it is observed that $\mathrm{H_{ud}}(j\omega)$ is replaced by unity. The reasons for this modification are the fact that the undelayed part of the plant consists of loss and gain coefficients, and in the steady-state gain and loss are in equilibrium and cancel out. Thus, the dynamics of the system H_p is replaced by a pure delay term $e^{-j\omega T'}$. Also, as Figs. 12 and 13 are compared, H_c is moved inside the Smith predictor loop, and this is to avoid influencing the original gain and loss of the main cavity. After these modifications, the transfer function of the modified Smith

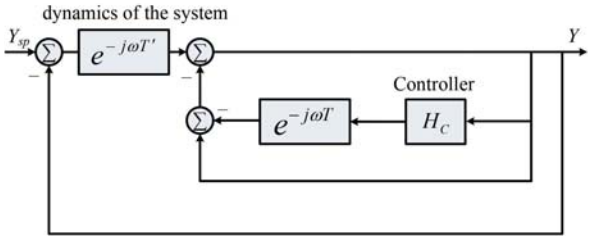

Fig. 13. Block diagram of the modified Smith predictor technique system applied to the FOPO system.

predictor becomes

$$H(\omega) = \frac{e^{-j\omega T'}}{2 - H_c e^{-j\omega T} + e^{-j\omega T'}}. \tag{5}$$

In case there is no model error $T = T'$, and $H_c = 1$ the transfer function reduces to

$$H(\omega) = \frac{e^{-j\omega T'}}{2}. \tag{6}$$

This shows that the modified structure is capable of eliminating the delay term from the characteristic equation. Moreover, H_c can be applied to compensate unpredicted losses inside the feedback loop of Smith predictor, as discussed in Section VI.

Figs. 14 and 15 show the experimental implementation and the equivalent linear model of the Smith predictor for the FOPO system, respectively. In this model, R_i denotes the connection and propagation losses related to ith fiber, T_{Li} represents the propagation delay of ith fiber, c_i, and d_i are the throughput and cross-path coupling ratios of ith optical coupler, R_{pi} indicates the insertion and polarization misalignment loss of ith polarization controller, T_2 represents the propagation delay of HNLF 2, R_{f2} is the insertion loss of HNLF 2, and G_c represents the controller gain. The required gain is provided by an Erbium-doped fiber amplifier (EDFA). Polarization controllers (PC), PC1 and PC2, ensure the superposition of the pump and signal polarization states in the cavity to attain maximum nonlinear gain. Based on the block diagram of Fig. 15, the transfer function of the Smith predictor becomes

$$\begin{aligned} H_{\mathrm{Smith}} &= \frac{R_1 e^{-j\omega T_{L1}}}{1 + B_3 e^{-j\omega T_3'} - B_4 e^{-j\omega T_4'}} \\ B_3 &= G_c d_1 d_2 c_3 c_4 R_1 R_4 R_5 R_7 R_{p1} R_{f2} \\ B_4 &= d_1 d_2 d_3 d_4 R_1 R_4 R_6 R_7 R_{p2} \\ T_3' &= T_2 + T_{L1} + T_{L4} + T_{L5} + T_{L7} \\ T_4' &= T_{L1} + T_{L4} + T_{L6} + T_{L7}. \end{aligned} \tag{7, 8}$$

Figs. 14 and 15 show the experimental setup and block diagram of the FOPO after the application of Smith predictor. Based on this model and the transfer function of the Smith predictor derived in (7), the closed-loop transfer function of FOPO becomes

$$\begin{aligned} H(\omega) &= \frac{B_1 e^{-j\omega T_1'}}{1 + B_2 e^{-j\omega T_2'} + B_3 e^{-j\omega T_3'} - B_4 e^{-j\omega T_4'}} \\ B_1 &= c_1 c_2 R_1 R_2 \sqrt{G_{\mathrm{NL}}} R_{\mathrm{NL}} \\ B_2 &= d d_5 c_1 c_2 R_1 R_2 R_3 R_{\mathrm{NL}} \sqrt{G_{\mathrm{NL}}} = R_{\mathrm{cav}} \sqrt{G_{\mathrm{NL}}} \\ B_3 &= G_c d_1 d_2 c_3 c_4 R_1 R_4 R_5 R_7 R_{p1} R_{f2} \end{aligned} \tag{9}$$

$$\begin{aligned} B_4 &= d_1 d_2 d_3 d_4 R_1 R_4 R_6 R_7 R_{p2} \\ T_1' &= T_1 + T_{L1} + T_{L2} \\ T_2' &= T_1 + T_{L1} + T_{L2} + T_{L3} \\ T_3' &= T_2 + T_{L1} + T_{L4} + T_{L5} + T_{L7} \\ T_4' &= T_{L1} + T_{L4} + T_{L6} + T_{L7} \end{aligned} \tag{10}$$

where T_1 denotes the propagation delay of the HNLF 1, R_{NL} is the insertion loss of the HNLF 1 and BPF, and G_{NL} is the nonlinear gain due to FWM inside the HNLF 1. A closer look at the denominator of the transfer function shows that each exponential term is relevant to one of the loops of the structure of Fig. 14, as predicted by Mason's rule. For instance, $B_2 e^{-j\omega T'_2}$ is associated with the loop containing HNLF 1, L_1, L_2, and L_3 (loop 1). B_2 is the transmittance of the elements in this loop and T_2' is the total propagation delay in this loop. Similarly, $B_3 e^{-j\omega T'_3}$ is associated with the loop containing L_1, L_4, L_5, HNLF 2, and L_7 (loop 2), and $B_4 e^{-j\omega T'_4}$ is associated with the loop containing L_1, L_4, L_6, and L_7 (loop 3). After obtaining the closed-loop transfer function, in the next section the control algorithm to achieve single mode type behavior in the FOPO system is discussed.

VI. Control Algorithm

After the closed-loop system and the related transfer function are presented, the main problem of eliminating the redundant modes is tackled. An equation for the gain of the controller (G_c) and the delay elements T_2', T_3', and T_4' has to be found, such that only selected modes remain while the rest of the modes are filtered or eliminated. To achieve this, the goal is to amplify certain modes while cutting off others to create a significant difference in amplitude between successive modes, thus achieving single mode type behavior. To analyze the magnitude of the modes, the first step is to obtain the magnitude of the closed-loop transfer function in (9)

$$|H(\omega)|^2 = \frac{{B_1}^2}{\left|1 + B_2 e^{-j\omega T_2'} + B_3 e^{-j\omega T_3'} - B_4 e^{-j\omega T_4'}\right|^2}. \tag{11}$$

In the FOPO, to obtain steady-state oscillations, the closed-loop characteristic (denominator of (9)) is set to zero [14]

$$1 + B_2 e^{-j\omega T_2'} + B_3 e^{-j\omega T_3'} - B_4 e^{-j\omega T_4'} = 0. \tag{12}$$

After obtaining the magnitude of the transfer function and the condition of oscillation, the complex exponential terms of the denominator of (11), denoted by $D(j\omega)$, are combined and expanded as follows:

$$\begin{aligned} &D(j\omega) \\ &= 1 + B_2^2 + B_3^2 + B_4^2 + 2B_2 \cos\left(\omega T_2'\right) + 2B_3 \cos\left(\omega T_3'\right) \\ &\quad -2B_4 \cos\left(\omega T_4'\right) + 2B_2 B_3 \cos\left(\omega\left(T_3' - T_2'\right)\right) \\ &\quad -2B_3 B_4 \cos\left(\omega\left(T_4' - T_3'\right)\right) - 2B_2 B_4 \cos\left(\omega\left(T_4' - T_2'\right)\right) \\ &= 1 + B_2^2 + B_3^2 + B_4^2 + 2B_2 \cos\left(\omega T_2'\right) + 2B_3 \cos\left(\omega T_3'\right) \\ &\quad -2B_4 \cos\left(\omega T_4'\right) + 2B_2 B_3 \big(\cos\left(\omega T_2'\right) \cos\left(\omega T_3'\right) \\ &\quad + \sin\left(\omega T_2'\right) \sin\left(\omega T_3'\right)\big) - 2B_3 B_4 \big(\cos\left(\omega T_4'\right) \cos\left(\omega T_3'\right) \\ &\quad + \sin\left(\omega T_4'\right) \sin\left(\omega T_3'\right)\big) - 2B_2 B_4 \big(\cos\left(\omega T_2'\right) \cos\left(\omega T_4'\right) \\ &\quad + \sin\left(\omega T_2'\right) \sin\left(\omega T_4'\right)\big). \end{aligned} \tag{13}$$

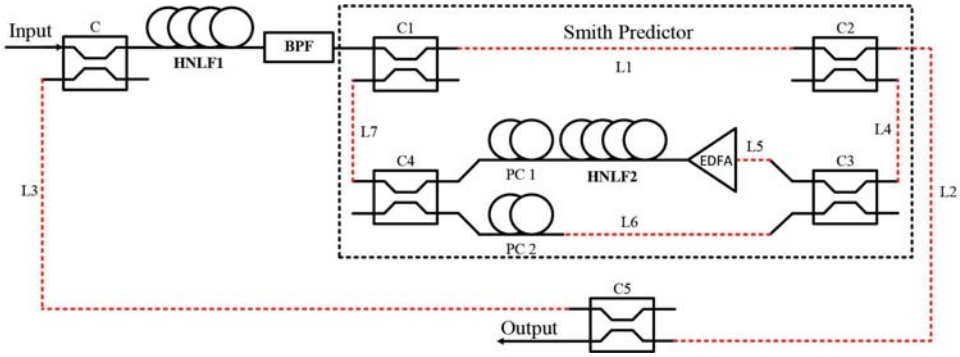

Fig. 14. Schematic of the experimental setup of the FOPO after the application of Smith predictor. PC, EDFA, BPF, and HNLF.

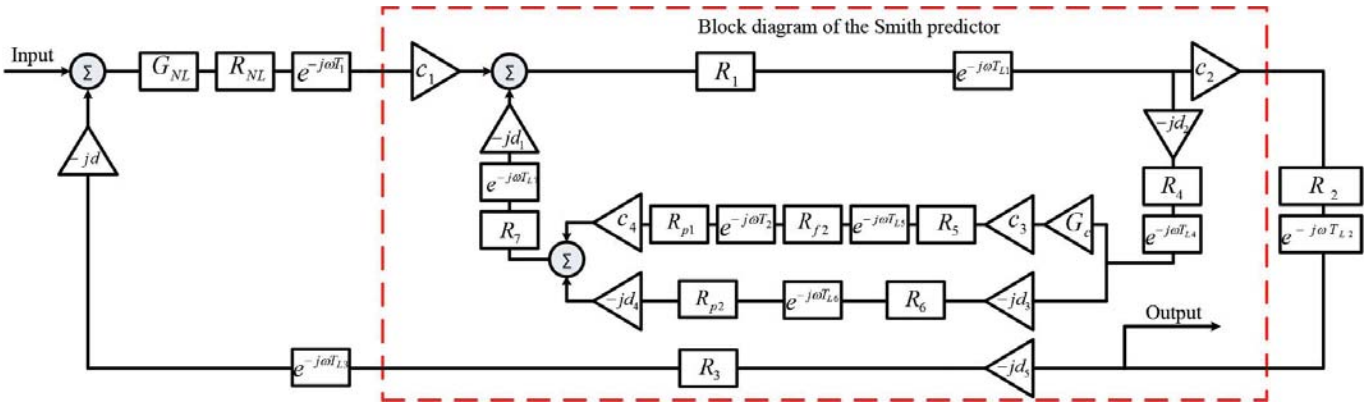

Fig. 15. Block diagram of the FOPO after the application of Smith predictor.

Examining (13), at a certain frequency $\omega_{\max}$, where $\cos(\omega_{\max} T_2') = \cos(\omega_{\max} T_3') = -1$, $\cos(\omega_{\max} T_4') = 1$ the magnitude of the transfer function becomes

$$|H(\omega_{\max})|^2 = \frac{{B_1}^2}{(1 - B_2 - B_3 - B_4)^2}. \tag{14}$$

At this frequency, the denominator of (11) will be minimum while the magnitude of the transfer function will be at maximum. Therefore, the mode which exists on the frequency $\omega_{\max}$ will be at maximum amplitude compared with the other modes. The goal is to amplify the amplitude of the mode at $\omega_{\max}$ even further to create a major separation between the dominant mode at $\omega_{\max}$ and the other successive modes. To achieve this goal, the condition of oscillation at $\omega_{\max}$ is $1 - B_2 - B_3 - B_4 = 0$. Substituting the value of B_2 from (10), and separating the linear and nonlinear parts, the oscillation condition reduces to

$$\sqrt{G_{\mathrm{NL}}} = \frac{1 - B_3 - B_4}{R_{\mathrm{cav}}}. \tag{15}$$

The nonlinearity of the parametric amplification behaves in a way that, as the output power increases, the nonlinear gain decreases. Therefore, to achieve the highest output power at frequency $\omega_{\max}$, the nonlinear gain must be at its minimum value $G_{\mathrm{NL}} = 1$. Setting $G_{\mathrm{NL}} = 1$, (15) is written as

$$1 - R_{\mathrm{cav}} - B_3 - B_4 = 0. \tag{16}$$

If (16) is achieved, the output power at $\omega_{\max}$ will be at the maximum possible value. Since B_4 and R_{cav} are constant values, the only adjustable parameter, to ensure that (16) holds, is B_3. B_3 in (9), can be written as $B_3 = G_c B_3'$, where $B_3' = d_1 d_2 c_3 c_4 R_1 R_4 R_5 R_7 R_{p1} R_{f2}$. Therefore, the gain of the controller which exists in B_3 has to be adjusted. Substituting B_3 in (16) the optimum controller gain G_{copt}, that results in the maximum output power restricted by nonlinearity, is obtained as

$$G_{\mathrm{copt}} = \frac{1 - R_{\mathrm{cav}} - B_4}{B_3'}. \tag{17}$$

If a certain mode is at the maximum allowable power while other modes are filtered out, then it is considered as a dominant mode in the frequency spectrum of the laser and the other modes can be neglected. Thus, the laser experiences a single mode type of behavior. In addition to the boosting, achieved by tuning the controller gain, there are tunable delay elements that affect the filtering features of the controller. As discussed in previous sections closely packed longitudinal modes originate from the time delay associated with the HNLF 1 (T_1), and the solution applied to eliminate this delay is based on adding another time delay (T_2) in the form of inner feedback loop. In an ideal theoretical case, there is no model error $T_2' = T_3'$, and $T_4' = 0$. In this case, as guaranteed by the Smith predictor method, the delay elements are eliminated from the characteristic equation and the longitudinal modes are completely filtered out. However in practice, it is impossible to achieve $T_2' = T_3'$, and $T_4' = 0$. Therefore, the longitudinal modes are not eliminated utterly, but are filtered significantly due to the presence of $\cos(\omega(T_3' - T_2'))$, and $\cos(\omega T_4')$ terms in (13). In our experiment, the first term generates a filter with FSR in the order of GHz and the second term has FSR of tens of MHz. After this point, the filters related to these terms are referred to as the GHz and MHz filters, respectively. Combination of these filters and the boosting

TABLE I
DEFINITIONS AND TYPICAL VALUES OF THE PARAMETERS USED FOR NUMERICAL ANALYSIS OF THEORETICAL RESULTS

Parameters	Definitions	Numerical Analysis
c_i	Throughput coupling coefficient of i^{th} coupler	0.7
d_i	Cross-path coupling coefficient of i^{th} coupler	0.7
R_i	Loss associated with i^{th} connecting fiber	1
R_{fi}	Loss associated with i^{th} HNLF	0.955
R_{pi}	Loss associated with polarization misalignment of the i^{th} polarization controller	1
G_c	Gain of the controller	variable
L_{HNLFi}	Length of i^{th} HNLF	$L_{HNLF1} = 1002.5$, $L_{HNLF2} = 1000.11$
L_i	Length of i^{th} connecting fiber	2.5 m

effect of the controller gain results in amplification of certain modes while attenuating other modes, thus creating dominant modes. In Section VII, these results are numerically analyzed with the parameters extracted from an experimental setup.

VII. NUMERICAL ANALYSIS

To numerically analyze the transfer function of the FOPO after the application of the Smith predictor, the transfer function of (9) with appropriate parameters extracted from the experimental setup is used. To include the nonlinearity of parametric amplification, the method introduced in [16] is applied. In this method, the denominator of (9) is set to zero. Then, the linear and nonlinear parts of the denominator are separated and their intersection is used to determine the nonlinear gain and output power at each frequency. Table I shows the definitions and typical values of the parameters used for numerical analysis. The nonlinear medium (HNLF1) is a HNLF with the propagation length of 1002.5 m and the nonlinearity coefficient of $\gamma = 13$ W^{-1}km^{-1}. The length of each of the connecting fibers is 2.5 m, and the dispersion coefficients are $\beta_2 = -10^{-28}$ s^{2}m^{-1} and $\beta_4 = 1.45 \times 10^{-55}$ s^{4}m^{-1}. The pump and signal are at the wavelengths $\lambda_p = 1557$ nm and $\lambda_s = 1568$ nm, respectively. The dispersion coefficients, and the pump and signal wavelengths are applied to determine the phase-mismatch parameter, which is used to obtain the nonlinear gain and phase shift [16]. It is assumed that all the optical couplers are 50/50, thus the numerical value of all the coupling ratios for electric field are 0.7. The length of HNLF2 is 1000.11 m, thus the length difference between loop 1 and loop 2 is 11 cm. The power loss coefficient is assumed to be 1.5 dB/km for the HNLFs and 0.2 dB/km for the connecting fibers. Therefore, the loss coefficients would be $R_{f1} \cong R_{f2} = 0.955$ for the HNLFs, and $R_i \cong 1$ for the connecting fibers.

Based on the values chosen in this analysis the cosine terms in (13) are divided to three major groups. First group consists of $\cos(\omega T_2')$, $\cos(\omega T_3')$, $\cos(\omega(T_4' - T_2'))$, and $\cos(\omega(T_4' - T_3'))$ with the frequency period of 200 kHz. The $\cos(\omega T_4')$ with frequency period of 20 MHz is in the second group and the third group is the $\cos(\omega(T_3' - T_2'))$ term with frequency period of 1.8 GHz. The last two cosine terms filter out the longitudinal modes generated by the first group. The last two terms, form the GHz and MHz filters introduced in Section VI.

Fig. 16(a) and (d) shows the transfer function as the controller gain is increased, or equivalently $G_c \rightarrow (1 - R_{\text{cav}} - B_4/B_3')$. As the controller gain is increased, the difference between maximum and minimum of the transfer function is increased, and unwanted modes are eliminated. When $G_c = 1$ this difference is 15 dB, but when G_c is increased to 2.14, the difference is more than 27 dB. This clearly illustrates how certain modes can be boosted by tuning the controller gain. The filtering effect of the $\cos(\omega(T_3' - T_2'))$ term (GHz filter) is clearly observed in Fig. 16(d). FSR of this filter is 1.8 GHz that results from the 11 cm path length difference between loop 1 and loop 2. Thus, by controlling the path length difference or equivalently the propagation delay difference, FSR can be tuned. In addition to this filter, there is another filter with FSR of 20 MHz (MHz filter). To obtain better understanding of the effect of 20 MHz filter on suppression of the longitudinal modes, only one period of the GHz filter is depicted. Fig. 16(b) and (e) shows one period of the transfer function for different values of the controller gain. When $G_c = 1$ the difference between amplitude of the successive 20 MHz modes is 0.2 dB, but when $G_c = 2.14$, this difference is 1 dB. In addition, the number of modes is reduced from 50 to 30, in the span of 1 GHz. As predicted by the transfer function of (13), a closer look at the 20 MHz mode reveals that 200 kHz modes are not completely eliminated. Fig. 16(c) and (f) shows filtered longitudinal modes in the vicinity of the dominant mode of the MHz filter for different values of the controller gain. While the controller gain is increased from 1 to 2.14, most of the 200 kHz modes are eliminated and the difference between the amplitude of the successive 200 kHz modes is increased from 0.2 to 1.2 dB. In conclusion, by setting the controller gain to 2.14, the number of the dominant modes reduces and the difference between the amplitude of the successive modes is increased.

VIII. EXPERIMENTAL RESULTS

A series of experiments were conducted using the setup shown in Fig. 14. FSRs of the GHz and MHz filter are set to 1.8 GHz and 20 MHz, respectively. As numerical analysis implied, increasing the gain of the controller leads in enhancement of the maximum to minimum ratio and the difference between the amplitude of the successive modes. To confirm this experimentally, an EDFA is applied to provide gain inside loop 2. Fig. 17(a) shows the RF spectrum of the output of FOPO before and after the application of the Smith predictor. It is demonstrated that the modes are drastically suppressed by the filtering effect of the Smith predictor. Peaks are generated at every 1.8 GHz due to the difference

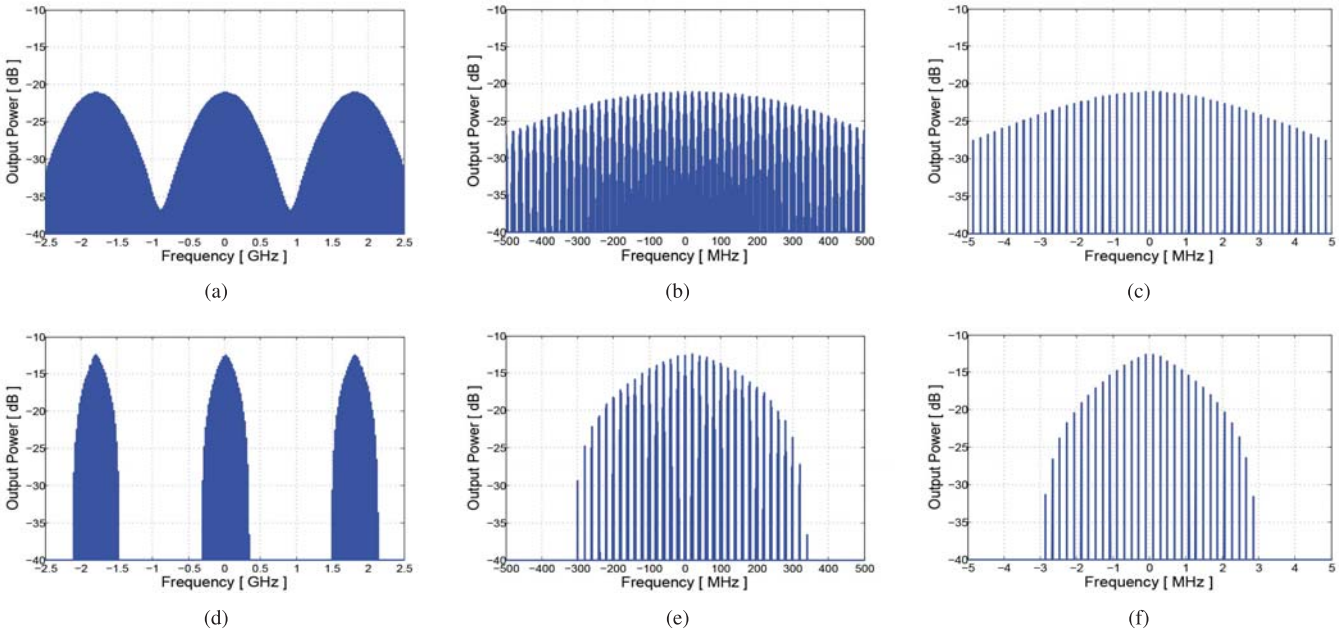

Fig. 16. Comparison of the transfer function for different values of the controller gain. As $R_{\text{cav}} + B_3 + B_4$ approaches 1, the central mode is amplified while the other modes are eliminated. (a) $R_{\text{cav}} + B_3 + B_4 = 0.75$ and $G_c = 1$. (b) $R_{\text{cav}} + B_3 + B_4 = 0.75$ and $G_c = 1$. (c) $R_{\text{cav}} + B_3 + B_4 = 0.75$ and $G_c = 1$. (d) $R_{\text{cav}} + B_3 + B_4 = 0.9995$ and $G_c = 2.14$. (e) $R_{\text{cav}} + B_3 + B_4 = 0.9995$ and $G_c = 2.14$. (f) $R_{\text{cav}} + B_3 + B_4 = 0.9995$ and $G_c = 2.14$.

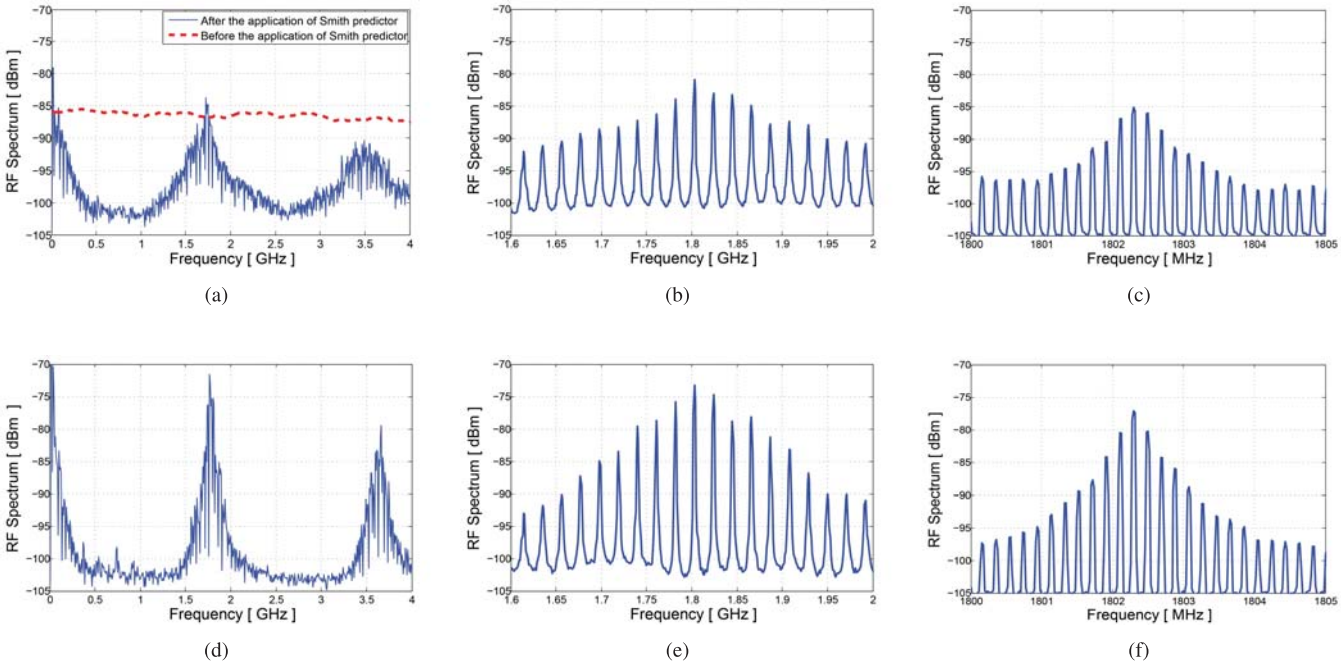

Fig. 17. Experimental measurement of RF spectrum of the Smith predictor enhanced FOPO with and without controller gain. (a) RF spectrum of FOPO with and without the Smith predictor. Controller gain is not applied. (b) RF spectrum of the Smith predictor enhanced FOPO. Controller gain is not applied. (c) RF spectrum of the Smith predictor enhanced FOPO. Controller gain is not applied. (d) RF spectrum of the Smith predictor enhanced FOPO. Controller gain is applied. (e) RF spectrum of the Smith predictor enhanced FOPO. Controller gain is applied. (f) RF spectrum of the Smith predictor enhanced FOPO. Controller gain is applied.

between the lengths of HNLF 1 and HNLF 2 while the maximum mode suppression, in the span of 1.8 GHz, is between 15 and 20 dB. The suppression level can be elevated by increasing the controller gain. Fig. 17(a) and (d) show two periods of the output spectrum for different values of gain. As gain is increased, the central modes are boosted and the difference between maximum and minimum of the transfer function is increased from 17 to 33 dB. Fig. 17(b) and (e) show the main peak of the transfer function as the EDFA gain is increased. As predicted by the numerical analysis, the 20 MHz modes exist but they are filtered by the GHz filter. The peak of the transfer function is increased from -84 to -73 dBm, which shows 11 dB enhancement of the central mode. In addition, the difference between the amplitude of the successive 20 MHz modes is increased from 1.2 to 2 dB. In agreement with predictions of the numerical analysis, a closer look at the main 20 MHz mode makes it clear that 200 kHz modes still exist. Fig. 17(c) and (f) show

the main 20 MHz mode as the EDFA gain is increasing. The peak of the transfer function is increased from -85 to -77 dBm which shows 8 dB enhancement of the central mode. Moreover, the difference between the amplitude of the successive 200 kHz modes is increased from 1.1 to 2 dB.

IX. Conclusion

In this brief, a closed-loop control method based on modified Smith predictor is proposed to suppress the longitudinal modes of a FOPO. To achieve this, a quasi-linear model for the operation of the FOPO is introduced and based on this model the transfer function of the FOPO cavity is derived. Then, applying simple components such as optical couplers and delay elements the control algorithm is developed to reduce the number of the longitudinal modes. To verify the validity of the results, the closed-loop system is experimentally implemented, where the experimental results show significant improvement in terms of mode suppression and tunability, thus confirming the effect of the Smith predictor controller on the system. It is observed that the number of longitudinal modes can be reduced by two to three orders of magnitude. The proposed structure is applicable to arbitrary wavelengths, thus is considered as a prominent candidate to suppress longitudinal modes at unconventional wavelengths (e.g., 2–5 μm).

References

[1] J. Hansryd, P. Andrekson, M. Westlund, J. Li, and P.-O. Hedekvist, "Fiber-based optical parametric amplifiers and their applications," *IEEE J. Sel. Topics Quantum Electron.*, vol. 8, no. 3, pp. 506–520, May/Jun. 2002.

[2] M. E. Marhic, *Fiber Optical Parametric Amplifiers, Oscillators and Related Devices*, 1st ed. Cambridge, U.K.: Cambridge Univ. Press, 2007.

[3] M. E. Marhic, K. K.-Y. Wong, L. G. Kazovsky, and T.-E. Tsai, "Continuous-wave fiber optical parametric oscillator," *Opt. Lett.*, vol. 27, no. 16, pp. 1439–1441, Aug. 2002.

[4] Y. Q. Xu, S. G. Murdoch, R. Leonhardt, and J. D. Harvey, "Widely tunable photonic crystal fiber fabry-perot optical parametric oscillator," *Opt. Lett.*, vol. 33, no. 12, pp. 1351–1353, Jun. 2008.

[5] O. Svelto and D. Hanna, *Principles of Lasers*. New York, NY, USA: Plenum Press, 1998.

[6] S. Yang, X. Xu, Y. Zhou, K. Cheung, and K. Wong, "Continuous-wave single-longitudinal-mode fiber-optical parametric oscillator with reduced pump threshold," *IEEE Photon. Technol. Lett.*, vol. 21, no. 24, pp. 1870–1872, Dec. 15, 2009.

[7] Y. Zhou, K. K. Y. Cheung, S. Yang, P. C. Chui, and K. K. Y. Wong, "Widely tunable picosecond optical parametric oscillator using highly nonlinear fiber," *Opt. Lett.*, vol. 34, no. 7, pp. 989–991, Apr. 2009.

[8] J. Liu, J. Yao, J. Yao, and T. H. Yeap, "Single-longitudinal-mode multiwavelength fiber ring laser," *IEEE Photon. Technol. Lett.*, vol. 16, no. 4, pp. 1020–1022, Apr. 2004.

[9] X. Cheng, P. Shum, C. H. Tse, J. L. Zhou, M. Tang, W. C. Tan, *et al.*, "Single-longitudinal-mode erbium-doped fiber ring laser based on high finesse fiber Bragg grating Fabry-Pérot etalon," *IEEE Photon. Technol. Lett.*, vol. 20, no. 12, pp. 976–978, Jun. 15, 2008.

[10] C.-H. Yeh, T. T. Huang, H.-C. Chien, C.-H. Ko, and S. Chi, "Tunable S-band erbium-doped triple-ring laser with single-longitudinal-mode operation," *Opt. Exp.*, vol. 15, no. 2, pp. 382–386, Jan. 2007.

[11] O. J. M. Smith, "A controller to overcome dead time," *ISA J.*, vol. 6, no. 2, pp. 28–33, 1959.

[12] G. Agrawal, *Nonlinear Fiber Optics*. San Diego, CA, USA: Academic Press, 2007.

[13] J. M. Senior, *Optical Fiber Communications, 3/E*. Upper Saddle River, NJ, USA: Pearson Education, 2009.

[14] A. Gelb and W. Vander Velde, *Multiple-Input Describing Functions and Nonlinear System Design*, New York, NY, USA: McGraw-Hill, 1968.

[15] D. Rabus, *Integrated Ring Resonators: The Compendium*. New York, NY, USA: Springer-Verlag, 2007.

[16] A. Salehiomran and M. Rochette, "A nonlinear model for the operation of fiber optical parametric oscillators in the steady state," *IEEE Photon. Technol. Lett.*, vol. 25, no. 10, pp. 981–984, May 15, 2013.

[17] D. Seborg, T. Edgar, and D. Mellichamp, *Process Dynamics and Control*. New York, NY, USA: Wiley, 2003.